Accounting for variability in ULF wave radial diffusion models

Article

Published Version

It is advisable to refer to the publisher's version if you intend to cite from the work. See Guidance on citing.

www.reading.ac.uk/centaur

CentAUR

Central Archive at the University of Reading

Reading's research outputs online

Key Points:
- Ensemble numerical experiments of radial diffusion are performed using stochastic parameterization of diffusion coefficients
- When reasonable temporal and spatial variability of diffusion is included, the temporal evolution of phase space density changes
- Diffusion depends on temporal and spatial scales of variability, and the size and shape of the distribution of diffusion coefficients

Supporting Information:
- Supporting Information S1
- Figure S1
- Figure S2
- Figure S3
- Figure S4
- Figure S5
- Figure S6

Correspondence to:
R. L. Thompson,
r.l.thompson@pgr.reading.ac.uk

Accounting for Variability in ULF Wave Radial Diffusion Models

R. L. Thompson[1] iD, C. E. J. Watt[2] iD, and P. D. Williams[2] iD

[1]Department of Mathematics and Statistics, University of Reading, Reading, UK, [2]Department of Meteorology, University of Reading, Reading, UK

Abstract Many modern outer radiation belt models simulate the long-time behavior of high-energy electrons by solving a three-dimensional Fokker-Planck equation for the drift- and bounce-averaged electron phase space density that includes radial, pitch-angle, and energy diffusion. Radial diffusion is an important process, often characterized by a deterministic diffusion coefficient. One widely used parameterization is based on the median of statistical ultralow frequency (ULF) wave power for a particular geomagnetic index Kp. We perform idealized numerical ensemble experiments on radial diffusion, introducing temporal and spatial variability to the diffusion coefficient through stochastic parameterization, constrained by statistical properties of its underlying observations. Our results demonstrate the sensitivity of radial diffusion over a long time period to the full distribution of the radial diffusion coefficient, highlighting that information is lost when only using median ULF wave power. When temporal variability is included, ensembles exhibit greater diffusion with more rapidly varying diffusion coefficients, larger variance of the diffusion coefficients and for distributions with heavier tails. When we introduce spatial variability, the variance in the set of all ensemble solutions increases with larger spatial scales of variability. Our results demonstrate that the variability of diffusion affects the temporal evolution of phase space density in the outer radiation belt. We discuss the need to identify important temporal and length scales to constrain variability in diffusion models. We suggest that the application of stochastic parameterization techniques in the diffusion equation may allow the inclusion of natural variability and uncertainty in modeling of wave-particle interactions in the inner magnetosphere.

Plain Language Summary The Van Allen outer radiation belt is a region in near-Earth space containing mostly high-energy electrons trapped by the Earth's geomagnetic field. It is a region populated by satellites that are vulnerable to damage from the high-energy environment. Many modern radiation belt models simulate the behavior of the high-energy electrons with a diffusion model, which describes how electrons spread out from areas of higher concentration to areas of lower concentration. An important process in these models is radial diffusion, driven by ultralow frequency (ULF) waves, where electrons are drawn from the outer boundary and accelerated toward Earth, or pushed away from the outer radiation belt and lost to interplanetary space. Radial diffusion is generally characterized by a parameter that provides a single output from the specified inputs and does not allow for any variability in the physical process. In this study we present a series of numerical experiments on radial diffusion, which allow for natural variability in both time and space and see how modeling of radial diffusion is impacted. Our results find that better understanding of temporal and spatial variations of ULF wave interactions with electrons, and being able to characterize these variations to a good level of accuracy, is vital to produce a robust description of radial diffusion over long timescales in the outer radiation belt.

1. Introduction

The Van Allen outer radiation belt is a typically quiescent torus-shaped region in near-Earth space between 13,000 and 40,000 km radial distance consisting mainly of electrons between 100s of keV and multiple MeV trapped by the Earth's geomagnetic field. Protons are also present and modeled in the radiation belts (Vacaresse et al., 1999), but here we focus on the high-energy electron population. The behavior of electrons in the outer radiation belt is affected by multiple processes, some of which are immediate responses to solar wind forcing, whereas some are more indirect energy pathways involving energy stored in the substorm cycle. Numerical modeling is a powerful tool to provide deep understanding of the behavior of the outer

radiation belt, allowing us to quantify the effects of different processes (e.g., Glauert et al., 2014; Reeves et al., 2012; Shprits et al., 2008).

From a more practical standpoint, the ability to model these physical processes is becoming increasingly important as Earth becomes more dependent on space-based technologies. As of 31 March 2020 there were 135 satellites operating in medium Earth orbit (MEO; 2,000–35,786 km) and 554 in geostationary orbit (GEO; 35,786 km), therefore operating in the heart of the belt (https://www.ucsusa.org). Outer radiation belt electrons can be hazardous to these spacecraft, but there are insufficient in situ measurements available to monitor the radiation environment directly. There remains a pressing need to develop accurate models of the outer radiation belt for operational purposes in addition to promoting further physical understanding.

One effective method to study the dynamics of the outer belt electrons is to model the evolution of electron phase space density (PSD) $f(M, J, \Phi; t)$ by a Fokker-Planck equation as a function of the three adiabatic invariants and time (Schulz & Lanzerotti, 1974). Here M, J, and Φ are the first, second, and third adiabatic invariants, respectively. It is helpful to consider Φ in terms of the adiabatic reference parameter L^*, defined by $L^* = 2\pi B_E R_E^2 / \Phi$ (Roederer, 1970). Since a first-principles model of wave-particle interactions in the outer radiation belt is intractable across its large volume and long timescales, all the physics within the outer radiation belt can be effectively described by diffusive processes. Each type of diffusion—pitch angle, energy, and radial—by each wave mode is described in the Fokker-Planck equation by a diffusion coefficient D_{ij}. A myriad of different wave-particle interactions is important for the radiation belts. For example, very low frequency (VLF) whistler mode chorus mediate energy diffusion (Thorne et al., 2013), whereas VLF whistler mode hiss (Lyons & Thorne, 1973; Meredith et al., 2007) and ULF electromagnetic ion cyclotron (EMIC) waves (Kersten et al., 2014) predominantly diffuse in pitch-angle and therefore contribute to loss. ULF wave-driven radial diffusion at Pc-5 frequencies is considered to be an important and effective mechanism to transport and accelerate relativistic electrons in the outer radiation belt (Elkington et al., 2003; Mann et al., 2013; Ozeke et al., 2017, 2018; Shprits et al., 2008).

In this paper we focus on radial diffusion as a result of ULF waves, which in the diffusion framework can be modeled as a straightforward one-dimensional problem. All of the physics is contained in the radial diffusion coefficient D_{LL}, which is proportional to ULF wave power. A wealth of data exists both on the ground and in space to calculate ULF wave power and construct D_{LL} (Dimitrakoudis et al., 2015; Li et al., 2017; Liu et al., 2016; Ozeke et al., 2012, 2014; Ukhorskiy et al., 2009). Empirical models formulate analytic expressions for D_{LL} from ULF wave power data over long timescales, aiming to capture the spatiotemporal evolution of D_{LL} in such a way that although rapid changes cannot be accurately captured, the long timescale behavior of the outer radiation belt may be adequately described (e.g., Ozeke et al., 2018). In this paper, we wish to highlight the numerical consequences of using different methods for modeling the temporal and spatial variability of D_{LL} with more realistic values that represent the underlying probability distribution of ULF wave power.

Many theoretical approximations exist for the radial diffusion coefficient D_{LL} based on a variety of assumptions and approximations (Ali et al., 2016; Birmingham, 1969; Cornwall, 1968; Elkington et al., 2003; Fälthammar, 1966, 1968; Fei et al., 2006; Lejosne et al., 2013; Liu et al., 2016; Schulz & Lanzerotti, 1974). All of these approximations are constrained by some statistical parameterization of ULF wave power obtained from many years of space or ground-based observations. The most widely used D_{LL} parameterizations in radiation belt models parameterize by the geomagnetic index K_p (Brautigam & Albert, 2000; Ozeke et al., 2012, 2014). These parameterizations are deterministic with a single output for each value of Kp.

Typical approaches in radiation belt modeling follow a classical parameterization approach whereby average or median D_{LL} values are used. These values only change when the fit parameters change, and therefore, there is a chance that the full range of variability of D_{LL} is not captured in this classical approach. In numerical weather prediction and climate modeling, classical parameterizations have proven to be insufficient. Instead, stochastic parameterizations are used to capture the whole distribution of behavior in underlying physical processes to yield improved results. Note that previous attempts to capture more realistic variability in ULF-mediated radial diffusion have used observations to recreate event-specific models of diffusion (Perry et al., 2005; Riley & Wolf, 1992; Tu et al., 2012). These types of study, although potentially more accurate, are limited to test cases with available data in space and time. We propose that in cases where direct data is

lacking, it is still possible to capture the full range of behavior in the problem using stochastic parameterizations (e.g., Watt et al., 2017), and we demonstrate a simple implementation of this technique in this paper.

Here we present a series of idealized numerical experiments of radial diffusion over a hypothetical period of constant geomagnetic activity. These experiments offer a proof of concept intended to explore the spatiotemporal impacts of including stochastic variability in comparison with the (Ozeke et al., 2014) ULF radial diffusion coefficients in the radial diffusion equation and highlight current deterministic model limitations. Any significant discrepancies between the deterministic and stochastic models should motivate further research questions to better understand the physical processes underlying ULF wave-driven radial diffusion to include in our models for improved accuracy. The remainder of this paper is structured as follows. Sections 2–4 describe the radial diffusion problem, implementation of stochastic parameterization, and setup and description of the idealized experiments, respectively. Section 3 presents the results from the numerical experiments. Section 4 discusses the impact of the results in the wider context of the outer radiation belt. Section 5 describes conclusions and remarks from this paper.

2. Modeling the Radial Diffusion Equation

We focus on the radial diffusion equation as a simplified approximate model of electron behavior in the outer radiation belt. Although the one-dimensional description of radial diffusion has successfully reproduced electron behavior during some events (e.g., Ozeke et al., 2018; Shprits et al., 2005), the diffusion framework itself is not always accurate. Previous studies have calculated radial diffusion coefficients directly in "event-specific" analysis (e.g., Ukhorskiy et al., 2009) and demonstrate that diffusion-based models can have difficulty accurately rendering event-specific dynamics (Ukhorskiy et al., 2009). Here, we intend these numerical experiments as a straightforward demonstration of the concept of stochastic parameterization. Radial diffusion is also a valid and important part of more complicated outer radiation belt models, where it is joined by diffusion processes in velocity space due to other wave modes. Over the long timescales studied in diffusion models, we observe that empirical models for D_{LL}, in whichever theoretical framework they are constructed, naturally have some uncertainty. Investigating the consequences of that uncertainty is our aim in this work.

In this demonstration we simplify the behavior of high-energy electrons in the outer radiation belt and focus on radial diffusion across Roederer L^* (Roederer, 1970), hereon denoted L. Here, the first and second adiabatic invariants, M and J, are conserved. The evolution of the distribution function of trapped particles $f(M, J, \Phi; t)$ can be related to the distribution function at time $t + \Delta t$ (without sources or sinks)

$$f(M, J, \Phi; t + \Delta t) = \int_{\Phi} f(\Phi - \phi, t)\Pi(\Phi - \phi, \phi, t)d\phi, \tag{1}$$

where $\Pi(\Phi - \phi, \phi, t)$ is the probability that a particle with an invariant shell coordinate $\Phi - \phi$ at time t will end up with coordinate Φ at time $t + \Delta t$. By Taylor expanding f, Π to first order in t on the left and second order in Φ in the integral, we obtain the one-dimensional Fokker-Planck equation

$$\frac{\partial f(M, J, \Phi)}{\partial t} = -\frac{\partial}{\partial \Phi}(D_{\Phi}f) + \frac{1}{2}\frac{\partial^2}{\partial \Phi^2}(D_{\Phi\Phi}f). \tag{2}$$

Here D_{Φ} and $D_{\Phi\Phi}$ are the first- and second-order Fokker-Planck diffusion coefficients, respectively. If we assume the following relation for D_{Φ}, the average change of Φ per unit time for one particle on the shell Φ during that time interval

$$D_{\Phi} = \frac{1}{2}\left(\frac{\partial D_{\Phi\Phi}}{\partial \Phi}\right) \tag{3}$$

and convert Φ into L, the evolution of the PSD of electrons may be modeled by a simplified radial diffusion equation in terms of L

$$\frac{\partial f(M, J, \Phi)}{\partial t} = L^2 \frac{\partial}{\partial L}\left(\frac{D_{LL}}{L^2}\frac{\partial f(M, J, \Phi)}{\partial L}\right). \tag{4}$$

For radial diffusion to be effective, a radial gradient in the PSD is required, which we assume here. A precipitation loss term is often also added to Equation 4, which is ignored here in the idealized case. Radial diffusion is considered across $L = 2.5$–6. Dirichlet and Neumann boundaries are imposed on the inner and outer boundaries, respectively:

$$f_{L = 2.5}(t) = f_{L = 2.5}(0) \quad \forall t, \tag{5}$$

$$\nabla f_{L = 6}(t) = 0 \quad \forall t. \tag{6}$$

In reality the gradient across the outer boundary will not be 0, and many radiation belt models either determine the outer boundary from electron flux data observed by spacecraft (e.g., Drozdov et al., 2017; Glauert et al., 2018; Shin & Lee, 2013) or use plasmasheet characteristics (Christon et al., 1988, 1991) and magnetic activity dependencies (Bourdarie & Maget, 2012) for analytic fits (Maget et al., 2015).

In Equation 4, D_{LL} represents the ULF wave radial diffusion coefficient. Constructed through a coordinate transform of the flux invariant diffusion coefficient, $D_{\Phi\Phi}$, D_{LL} is formally defined by (Roederer & Zhang, 2014)

$$D_{LL} = \frac{<(\Delta L)^2>}{\tau_d} \propto R_s^{-8} L^{10} (\Delta R_s/R_s)^2, \tag{7}$$

where R_s, $\Delta R_s/R_s$, and τ_d are the dipole-distortion parameter, its relative fluctuation, and the drift period, respectively. Here, $<>$ denotes the drift-average operator. In a realistic setting, R_s would be represented by a parameter that globally describes magnetospheric activity, such as Kp or ULF wave power. Application of different frameworks to describe large-scale fluctuations of electric and magnetic fields (e.g., Brautigam & Albert, 2000; Brautigam et al., 2005; Lejosne et al., 2013; Ozeke et al., 2012, 2014) employ different assumptions, but many ultimately require some estimate of the power spectral density of ULF fluctuations in electric and/or magnetic fields. We note that from Equation 7 and from theoretical estimates of D_{LL}, there are inherent minimum temporal scales on which D_{LL} is constructed: by definition D_{LL} is constructed for timescales longer than the drift period of the electrons, longer than a few periods of the ULF wave fluctuations, and of the same order or longer than the solar wind driving processes that induce the ULF fluctuations. In many cases, ULF power spectral density is estimated from observations over a period of at least an hour (see Ozeke et al., 2014), and so we employ this as the smallest timescale of variability in our study.

We consider as a deterministic reference model the empirical L and K_p parameterized D_{LL} presented by Ozeke et al. (2012, 2014). This model is a simplification of the theoretical analysis presented by Fei et al. (2006) and assumes that median ULF wave power is representative of expected ULF wave power. The most notable feature of this model is that the uncertainty in the statistical representation of ULF power spectral density has been quantified, allowing us to perform this demonstration using observationally derived constraints. Other models exist, which are similarly parameterized by Kp activity, with some following the same theoretical framework as Fei et al. (2006) (e.g., Brautigam et al., 2005) and others pursuing other frameworks (e.g., Lejosne et al., 2013), but all do not explicitly state and characterize the uncertainty in their models as in Ozeke et al. (2012, 2014). We note that the accuracy of the theoretical framework used to estimate D_{LL} is beyond the scope of this paper and direct the interested reader toward Lejosne (2019) for a thorough review of such frameworks. We reiterate that since the (Ozeke et al., 2014) empirical D_{LL} model contains explicit estimates of uncertainty, that makes it appropriate for use in our demonstration.

Since the azimuthal electric field radial diffusion coefficient, D_{LL}^E, typically dominates, in these idealized experiments we omit the compressional magnetic component and base our stochastic parameterization around the model for $D_{LL} = D_{LL}^E$, expressed per day by

$$D_{LL}^E = 2.16 \times 10^{-8} L^6 10^{0.217L + 0.461K_p}. \tag{8}$$

We describe in the following section how we implement our estimates of $D_{LL}^E(t)$, by perturbing Equation 8 in such a way as to recover a better representation of the underlying distribution of D_{LL}^E across a period of time.

We solve the radial diffusion equation using a modified Crank-Nicolson second-order finite difference scheme presented by Welling et al. (2011), which is semi-implicit and unconditionally stable:

$$
\frac{f_j^{n+1} - f_j^n}{\Delta t} = \frac{L_j^2}{2} \left[\frac{D_{j+\frac{1}{2}}n+\frac{1}{2}(f_{j+1}^n - f_j^n) - D_{j-\frac{1}{2}}n+\frac{1}{2}(f_j^n - f_{j-1}^n)}{(\Delta L)^2} \right.
$$
$$
\left. + \frac{D_{j+\frac{1}{2}}n+\frac{1}{2}(f_{j+1}^{n+1} - f_j^{n+1}) - D_{j-\frac{1}{2}}n+\frac{1}{2}(f_j^{n+1} - f_{j-1}^{n+1})}{(\Delta L)^2} \right], \tag{9}
$$

where $L_j = 2.5 + j\Delta L$, $t_n = n\Delta t$, $f_j^n = f(L_j, t_n)$, $D_j n + \frac{1}{2} = D_{LL}(L_j, t_{n+\frac{1}{2}})$ and $D_{LL} = \frac{D_{LL}}{L^2}$ for modeling simplicity. The chosen grid and time steps for our numerical experiments are $0.1L$ and 1 s, respectively, following extensive model verification of the numerical scheme to determine a suitable trade off between numerical error and computational cost for the experiments (see the supporting information).

3. Stochastic Parameterization

We suggest that the most physically intuitive method to implement stochastic parameterization is to focus efforts on the representation of the diffusion coefficient, since it is the variable that contains all the information about the wave-particle interaction. The diffusion coefficient parameterization has been shown to result in a large amount of variability, especially during storm times (Murphy et al., 2016). In this work, we choose a straightforward method to model $D_{LL}(L,t)$ that involves constructing a noisy temporal or spatial series that retains the key known properties of the distribution of D_{LL}. More sophisticated techniques, such as autoregressive moving average (ARMA) models, can be used to create spatiotemporal series of the diffusion coefficients with the appropriate autocorrelative properties. However, these rely on important characteristic scales of spatial and temporal variability that are not yet known.

We do, however, have access to some information constraining the expected distribution of D_{LL}. Bentley et al. (2018) found that the probability distribution of ground-based ULF wave power appears log-normal (LN). We infer from this that D_{LL} is also likely to be approximately LN; indeed, Ozeke et al. (2014) confirm that the distribution of D_{LL} in space is not Gaussian and is log-symmetric, since the interquartile range (IQR) is reported between one third and three times the median. Hence, it is appropriate to construct a noisy time series for D_{LL} by multiplying the median D_{LL} by a random LN noise factor ϵ, resulting in a time series that, when aggregated over a long period of time, reproduces the required LN distribution. If we constructed a noisy temporal or spatial series by adding Gaussian noise to the median D_{LL}, the resulting distribution of D_{LL} cannot be LN since it has the potential to include negative values of diffusion, which would also be difficult to interpret in this context.

To investigate the consequences of variability, we consider ensembles of numerical experiments. In each case we compute the solutions of the radial diffusion equation using Equation 9, where $D_{LL}(t)$ is separately constructed each time using the methods described below. Our recreations of $D_{LL}(t)$ do not alter the underlying Fokker-Planck diffusion theory but produce realizations of D_{LL} that better recover the underlying distribution of ULF power spectral density. Future work will seek to identify the most appropriate methods to model both the diffusion coefficient and its variability, but the straightforward methods we adopt here serve to illustrate the behavior of the radial diffusion equation when stochastic parameterization is adopted using known constraints.

4. Numerical Experiments

We consider radial diffusion under a constant state of low geomagnetic activity, with K_p fixed for 2 days. Although K_p is not typically constant over 2 days, we keep it fixed in these experiments in order to isolate the effects of the natural temporal and spatial variability that is concealed within the K_p parameterization. Any temporal changes to D_{LL} occur on timescales of hours in our experiments.
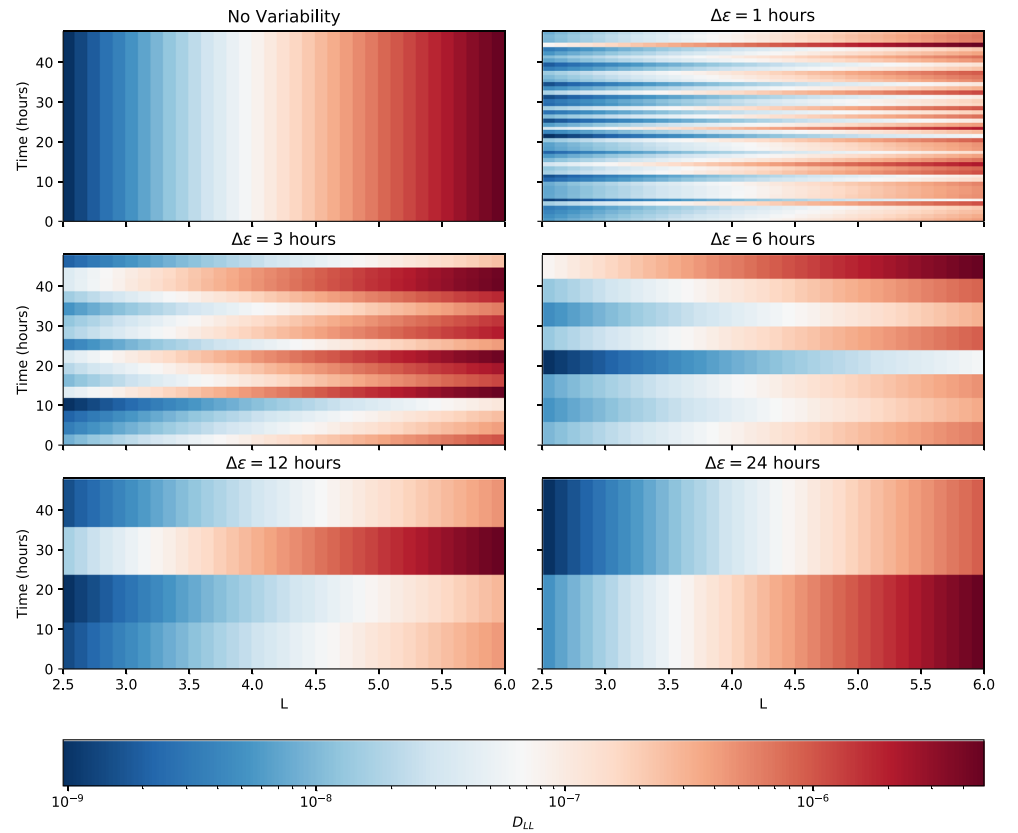
Figure 1. Example ensemble member D_{LL} time series shown for a range of temporal variability scales. In each case, the constant (Ozeke et al., 2014) deterministic D_{LL} is multiplied by a log-normal variability at the relevant hour of variability, constrained by the empirical model and ULF wave power observations, and persists until to the next hour of variability where the process is repeated. Examples are shown for variability temporal scales of 1, 3, 6, 12, and 24 hr, along with the constant D_{LL} with no variability. D_{LL} shown here has units s^{-1} in line with the 1 s time step used in our numerical scheme.

In each numerical experiment we run an ensemble with 250 ensemble members, providing a span of possible realizations of 48 hr D_{LL} time series resulting from the inclusion of a stochastic variability. Convergence testing of our numerical experiments (see the supporting information) demonstrates that 250 ensemble members is sufficient to realize the behavior of the experiment.

In all experiments we choose $K_p = 3$, corresponding to "unsettled" geomagnetic activity. Unsettled geomagnetic activity allows us to explore stochastic variabilities during periods where the radial diffusion coefficients are large enough to see changes after 48 hr. We also wish to avoid the illogical situation of having a very high level of geomagnetic activity while enforcing a constant outer boundary. For the demonstrations approximated in this paper, a compromise of $K_p = 3$ was felt to be appropriate. The initial PSD is chosen to provide a peak inside the computational domain as expected in the outer radiation belt, and a zero gradient at the outer boundary, for ease of computation in these illustrative experiments

$$f(M, J, \Phi; t = 0) = A\exp\left(-\frac{(L-\mu)^2}{2\sigma^2}\right) + \frac{1}{2}AB\left[erf(\gamma(L-\mu))+1\right], \tag{10}$$

where we have chosen $A = 9 \times 10^4$, $\mu = 4$, $\sigma = 0.38$, $B = 0.05$, and $\gamma = 5$ and erf is the error function. Such a profile is reasonable when compared to satellite observations (e.g., see Figures 1 and 2 in Boyd et al., 2018).

If one wanted to do the equivalent in L space (with a transformed diffusion equation), it suffices to use (Roederer & Zhang, 2014)
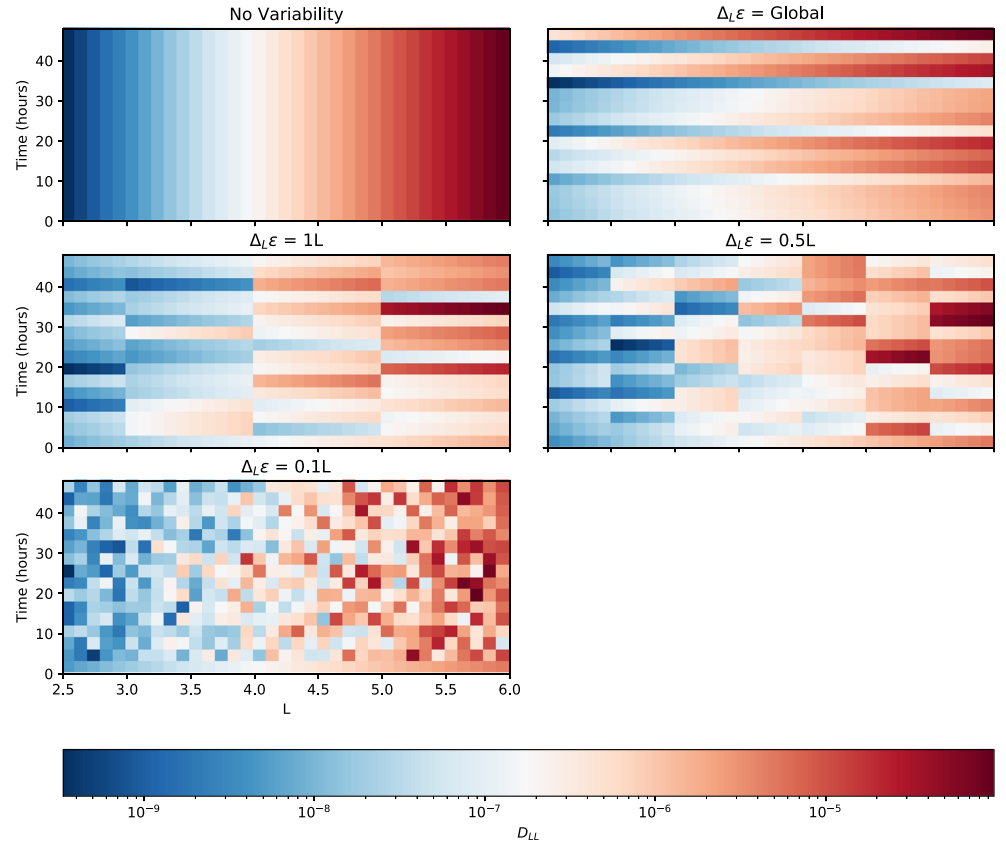
Figure 2. Example ensemble member D_{LL} time series shown for a range of spatial variability scales. In each case, every 3 hr the constant (Ozeke et al., 2014) deterministic D_{LL} is multiplied by log-normal variabilities on a variety of local spatial variability scales, constrained by the empirical model and ULF wave power observations, and persists for 3 hr where the process is then repeated. Examples are shown for variability spatial scales of $1L$, $0.5L$, and $0.1L$, along with the global variability case and constant D_{LL} with no variability. D_{LL} shown here have units s^{-1} in line with the 1 s time step used in our numerical scheme.

$$f(M, J, L; t = 0) = f(M, J, \Phi; t = 0) \times 2\pi B_E R_E^3 L^{-2}. \tag{11}$$

The initial PSD profile and proposed boundary conditions result in the expected radial diffusion process drawing PSD from central L toward both boundaries.

4.1. Experiment 1: Temporal Variability of D_{LL}

Our first experiment focuses on the temporal variation of D_{LL} across a range of timescales. We employ a simple method, where the D_{LL} in Equation 8 is multiplied by a random factor ϵ, which changes every Δt. The same factor ϵ is applied at each value of L in the model. The choice of distribution of ϵ is guided by the statistical analysis presented by Ozeke et al. (2014), who found that the IQR of observed wave power implies that D_{LL} lies between a third of and three times the model value 50% of the time. We use this information to control the variance of the noise. Combined with recent studies that suggest that ULF wave power spectral densities appear LN (Bentley et al., 2018), we construct a log-normally distributed variability with the following parameters:

$$\epsilon \sim LogNormal\left(\mu_N, \sigma_N^2\right), \tag{12}$$

where $(\mu_N, \sigma_N) = (0, \frac{2\log(3)}{1.34896})$ are the parameters of the normally distributed $\log(\epsilon)$. Note that for a normally distributed random variable, the IQR is approximately 1.34869 multiplied by the standard deviation. We consider variability $\Delta t = 1, 3, 6, 12$, and 24 hr, and example ensemble members for each of these cases are shown in Figure 1. They are effectively artificial representations of what might be observed in situ.

4.2. Experiment 2: Spatial Variability of D_{LL}

In Experiment 1, D_{LL} was constructed with perfect correlation across all L, with the same ϵ applied to all L-shells. This is one extreme of L spatial correlation, with the (Ozeke et al., 2014) D_{LL} scaling as a smooth, monotonically increasing profile. We hereon refer to this approach as *global* variability. However, we must consider that although the statistical profile of $D_{LL}(L)$ is smooth, individual cases of $D_{LL}(L,t)$ may be less smooth. In this experiment, we investigate how radial diffusion responds to a realized D_{LL}, which may vary on local spatial scales, and not necessarily be a smooth monotonically increasing function of L.

We now consider the log-normally distributed variability applied every 3 hr, comparing the global variability with local spatial correlation scales. We consider cases where D_{LL} varies independently on spatial scales of $1L, 0.5L$, and $0.1L$. Example ensemble members for each of these cases are shown in Figure 2. The final case denotes the other extreme where measures of $D_{LL}(L,t)$ are independent at all grid points, that is, that independent ϵ is applied at each grid point in L to create an ensemble of D_{LL} both spatially and temporally. We have retained temporal variability in this experiment to maintain our goal of creating D_{LL} time series that represent realistic values. Ground magnetometer ULF wave power measurements, and consequently D_{LL}, do not typically remain constant over 2 days (e.g., Olifer et al., 2019). Results from differing spatial variability scales can therefore be interpreted in conjunction with the 3-hourly temporal variability.

In a more physical realization, we would expect spatial correlations across L to be less crude and abrupt, and are likely to exhibit smoother variations with appropriate length scales. However, for the purpose of this demonstration, we have chosen the simplest way to apply spatial variability in the model to motivate the importance of understanding the spatial structure of radial diffusion across L.

4.3. Experiment 3: Width of the D_{LL} Probability Distribution

The empirical (Ozeke et al., 2014) D_{LL} parameterization is based on the median of statistical ULF wave power, and uncertainty in the parameterization has the multiplicative IQR $\left[\frac{1}{3}D_{LL}, 3D_{LL}\right]$ mentioned previously. We compare the IQR suggested by Ozeke et al. (2014) with larger and smaller IQRs, namely, $\left[\frac{1}{2}D_{LL}, 2D_{LL}\right]$, $\left[\frac{1}{6}D_{LL}, 6D_{LL}\right]$, and $\left[\frac{1}{10}D_{LL}, 10D_{LL}\right]$. Larger variances may be necessary if the variability of D_{LL} is not simply due to the variability in observed ground-based ULF power spectral density. Smaller variances have been considered to see the effect of an "improved" parameterization (i.e., one where the parameters are chosen in a way that minimizes the variance). In each of these cases, ensemble D_{LL} time series are formulated by applying variability globally across L every 3 hr, with the distribution of the variability LN.

4.4. Experiment 4: Shape of the D_{LL} Probability Distribution

Each experiment (1–3) utilized a log-normally distributed variability, chosen based on statistical studies of ULF wave power spectral densities parameterized by solar wind variables (Bentley et al., 2018). The IQR presented by Ozeke et al. (2014) describes the uncertainty in the deterministic parameterization, but we do not know how the D_{LL}s are distributed in a K_p-based model. Adopting the values and log-symmetric nature of the (Ozeke et al., 2014) IQR in order to preserve statistical averages (a zero mean and median in the logarithm), a range of log-symmetric distributions for the variability are tested. We consider log-uniform (LU), LN, log-Laplace (LL) and log-Cauchy (LC) distributions, which provides a set of distributions ranging from bounded to heavy tailed (for further information about each of these distributions, please see the supporting information). Since the heavy tailed distributions can easily produce variabilities resulting in a D_{LL} which is unrealistically many orders of magnitude larger than the deterministic solution, for this experiment we bound the variability by 3 orders of magnitude (i.e., the variability can increase/decrease D_{LL} up to a maximum/minimum of 3 orders of magnitude compared to the reference value). The respective probability density functions (PDFs) of the variability distributions are as follows:

$$f_{LU}(x) = \frac{I_{[e^a, e^b]}(x)}{x(b-a)}, \tag{13}$$

$$f_{LN}(x) = \frac{1}{x\sigma_N\sqrt{2\pi}}\exp\left(-\frac{(\ln x)^2}{2\sigma_N^2}\right), \tag{14}$$
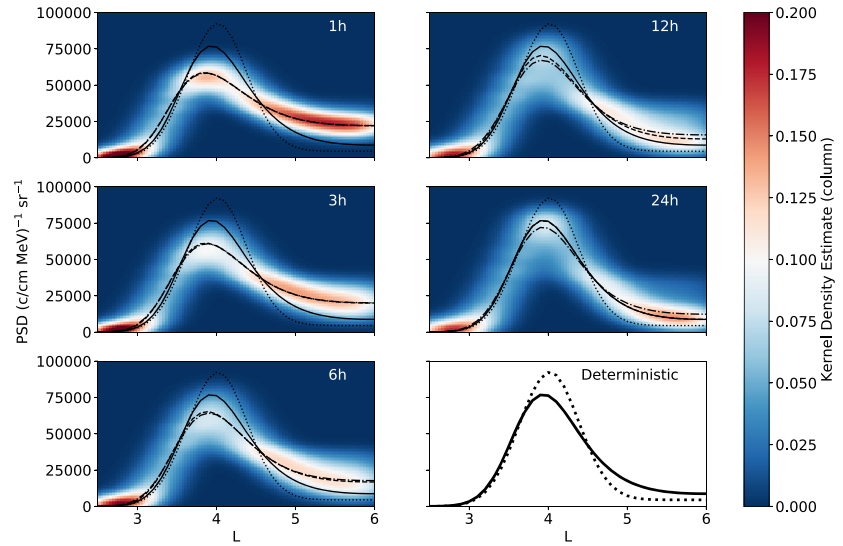
Figure 3. Ensemble results for the final PSD at the end of Experiment 1 for a range of temporal variability scales (1, 3, 6, 12, and 24 hr, respectively). The median (dashed), mean (dash-dot) ensemble profiles are shown, as well as the initial PSD profile (dotted) and the deterministic solution with constant deterministic D_{LL} (solid). Ensemble kernel density estimates of the resulting electron PSD are also shown.

$$f_{LL}(x) = \frac{1}{2\sigma_L x} \exp\left(-\frac{|\ln x|}{\sigma_L}\right),$$

(15)

$$f_{LC}(x) = \frac{1}{x\pi}\left[\frac{\sigma_C}{(\ln x)^2 + \sigma_C^2}\right]$$

(16)

for $x > 0$, where $I_{[,]}$ is the characteristic function. Here the quantities a, b, σ_N, σ_L, and σ_C are the parameters of the underlying uniform, normal, Laplace, and Cauchy distributions, respectively. The parameters were calculated from their corresponding cumulative density functions in order to preserve the IQR specified by Ozeke et al. (2014) (see the supporting information).

5. Results

The figures showcasing results for each experiment generally follow the same format. The initial PSD and resulting PSD from the constant deterministic D_{LL} are shown. By the log-symmetric nature of the D_{LL} probability distributions in each experiment, the constant deterministic D_{LL} is precisely the median diffusion coefficient from the ensemble and a natural reference for comparison. The mean diffusion coefficient is deliberated in section 6. There is no convention regarding which statistical measure is most appropriate in ensemble modeling (Knutti et al., 2010), and we have therefore shown two natural measures, the ensemble mean and median. By ensemble mean (median) PSDs, we imply the PSD profile resulting from taking the mean (median) across all ensemble members at each L, and not representing a specific member of the ensemble. The kernel density estimates (KDEs) of the ensembles are also shown. Kernel density estimation is a mathematical process of finding an estimate PDF of a random variable, inferring attributes of a population based on a finite data set. In the case of our ensembles, the contribution of each ensemble member value in L-PSD space is smoothed out into a region of space surrounding it. Aggregating each of these smoothed points provides an image of the overall ensemble structure and density function. Ensemble modes, another useful measure of the ensemble result, can be estimated from this density function (Kourentzes et al., 2014). In our figures KDEs shown are relative to each column, meaning that if a single L column were extracted, the result would be a PDF estimate of the PSD at that particular L. KDEs are therefore useful in an ensemble setting since they allow us to see where ensemble member solutions cluster in the phase space. In our estimates the KDEs are calculated over 100 bins.
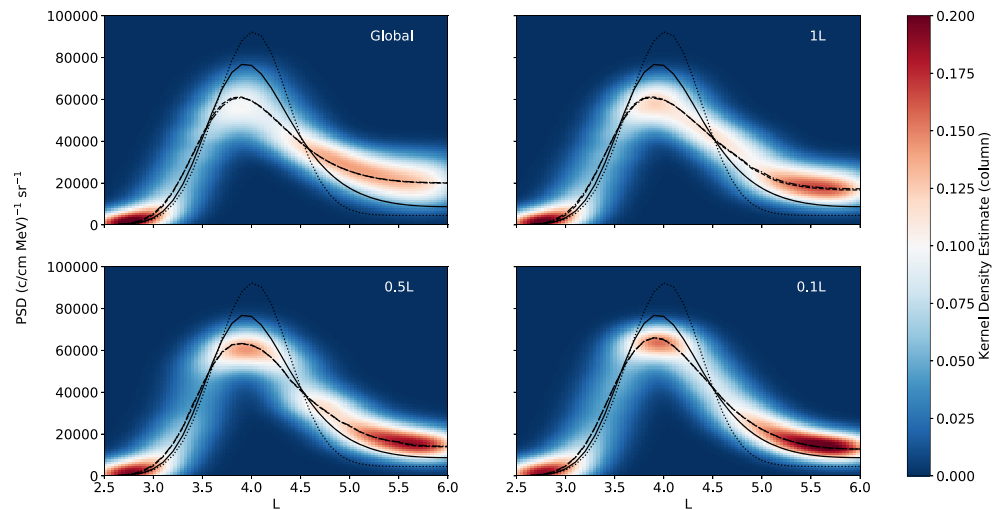
Figure 4. Ensemble results for the final PSD at the end of Experiment 2 for a range of spatial variability scales (global, 1*L*, 0.5*L*, and 0.1*L*, respectively). The description of lines and KDEs are as in Figure 3.

5.1. Experiment 1—Temporal Scales

Results of the ensembles for the variety of temporal variability scales are shown in Figure 3. For ensemble medians, inclusion of a LN variability results in more diffusion than the constant deterministic D_{LL} at all variability temporal scales less than 24 hr, with the magnitude of diffusion increasing as the temporal scale decreases. The ensemble median for a temporal variability of 24 hr is identical to the deterministic solution, suggesting that on long timescales, a deterministic parameterization of D_{LL} is sensible for a D_{LL} with daily variation. Results for the ensemble mean are similar, except we observe more diffusion than the constant D_{LL} at all temporal scales. This is unsurprising since the (Ozeke et al., 2014) D_{LL} is based on the median of log-symmetric distributions, where means are larger than medians. Therefore, the ensemble D_{LL} time series at all temporal scales will have a mean larger than both the deterministic approximation and ensemble median, resulting in more diffusion. An interesting result lies in the comparison of ensemble medians and means. On the most rapid temporal D_{LL} variability of 1 hr, results from the ensemble mean and median are identical. As the temporal variability becomes less rapid, both exhibit less diffusion, but the profiles separate with the ensemble median displaying increasingly less diffusion than the mean as it approaches the deterministic solution at daily variability.

Over all temporal variability scales, the occurrence of possible states in the set of all ensemble solutions spans similar regions. For the rapid 1 hr variability, the set of all solutions is more diffusive than the deterministic case. The deterministic solution becomes increasingly closer to the denser region of ensemble solutions with larger temporal scales, falling exactly in the region of highest probability for daily variation. We see that increasing the frequency of D_{LL} variability tends to a single mode solution in density, which is more diffusive than that produced by the deterministic model. Inclusion of the variability expressed by Ozeke et al. (2014) in their 3-hourly deterministic model produces a span of solutions, which vary greatly from the deterministic case at all *L*, most of which are more diffusive. The use of the median-based deterministic parameterization may therefore not be robust. When we allow the stochastic D_{LL} to vary daily, however, the deterministic solution fell exactly in the regions of highest probability, emphasizing again that the deterministic approximation is more suitable for a daily varying D_{LL}. When including variability, the deterministic parameterization frequently produces lower estimates of radial diffusion, so understanding the temporal variability of ULF wave power spectral density is important to know the extent of potential underestimation.

5.2. Experiment 2—Spatial Scales

Ensemble results for Experiment 2 are shown in Figure 4. We find that on average all spatial scales of variability result in similar levels of diffusion, but all exhibit more diffusion than the deterministic solution. In each case the ensemble means and medians are almost identical. Most importantly, we observe variance
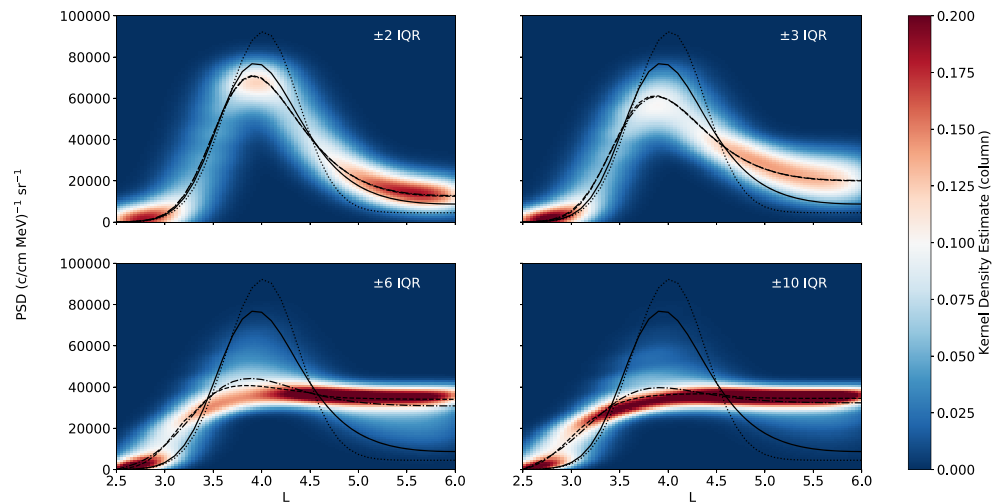
Figure 5. Ensemble results for the final PSD at the end of Experiment 3 for a range of log-normal variability IQRs (± 2, ± 3, ± 6, and ± 10 of the deterministic D_{LL}, respectively). The description of lines and KDEs are as in Figure 3.

reduction in the set of ensemble solutions as independence of D_{LL} measurements occurs on increasingly smaller spatial scales, with the distributions tending toward a single mode solution of diffusion similar to those exhibited by the ensemble median and mean. A smaller variance implies possibility of a stronger parameterization with reduced uncertainty. It is important to investigate instantaneous observations of ULF wave power across multiple latitudes to better understand spatial correlations and coherence across $L*$, since regions of independent power measurements could allow for better parameterizations of D_{LL}.

5.3. Experiment 3—Variance

Figure 5 shows the ensemble results for Experiment 3, with each variance expressed in terms of the variability IQR. It is evident that radial diffusion is very sensitive to the width of the variability distribution. Just doubling the multiplicative scaling of the IQR suggested by Ozeke et al. (2014) results in significantly more diffusion in both ensemble averages, reducing the peak in PSD by around 20,000. The shape of the distribution for the set of all ensemble solutions also drastically changes, with a large density of solutions tending to the asymptotic result controlled by the boundary conditions. Although a wider variability distribution equally allows for both significantly larger and smaller vales of D_{LL}, the radial diffusion equation is clearly heavily sensitive to the larger values that drive radial diffusion to significant levels beyond the deterministic approximation.

As seen in the other experiments, introduction of any variability regardless of its width results in more diffusion than the deterministic solution, when considering ensemble averages. However, if the uncertainty in the deterministic model were to have a slightly smaller multiplicative IQR of ± 2 the (Ozeke et al., 2014) D_{LL}, the variance of all ensemble solutions decreases significantly. With this smaller variance, the ensemble mean and median PSDs are closer to the deterministic model, which also falls within the set of ensemble solutions. This suggests that parameterization of ULF radial diffusion coefficients should prioritize variance reduction in order to be better representative of the underlying physical process, which draws upon the efficiency of binning by geomagnetic index K_p, from which most of the uncertainty arises (Ozeke et al., 2014).

5.4. Experiment 4—Underlying Distribution

Ensemble results for Experiment 4 are shown in Figure 6. Differences between the heavy and nonheavy tailed distributions are apparent in the ensemble medians. Although studies suggest that ground-based ULF power spectral density is LN when parameterized by solar wind variables (Bentley et al., 2018), the distribution of uncertainty in the K_p-based (Ozeke et al., 2014) model is not disclosed. If the distribution were to be heavy tailed or LU (which may be considered to have the heaviest tail as all values in the uniformly distributed component have equal chance of being sampled), we see more than double the median diffusion than for a log-normally distributed variability. For scenarios where the expected ULF wave power is not a
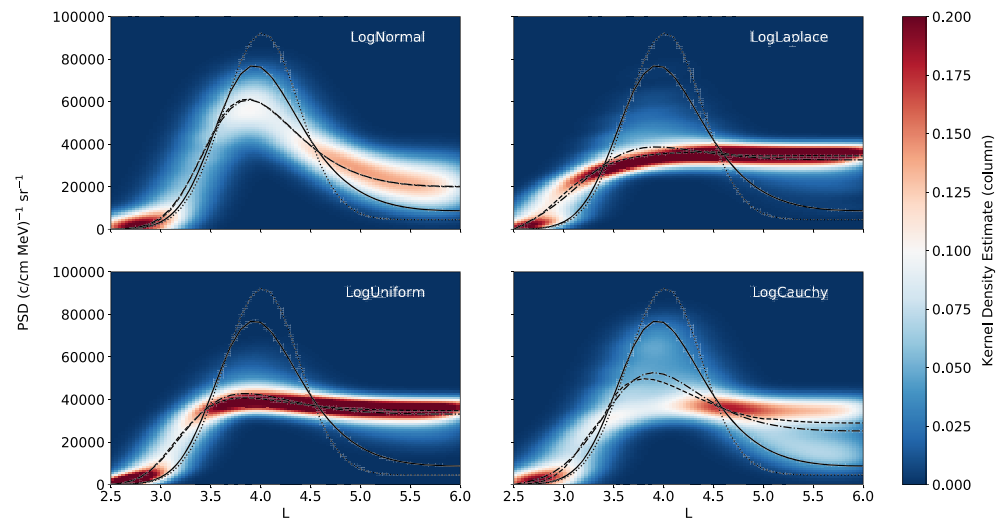
Figure 6. Ensemble results for the final PSD at the end of Experiment 4 for a range of variability probability distributions (Log-Normal, Log-Laplace, Log-Uniform, and Log-cauchy, respectively). The description of lines and KDEs are as in Figure 3.

statistical average, the assumed LN variability can exhibit as much diffusion as some of the heavy tailed variabilities, but this is more unlikely as shown in the KDEs. In any case, with the inclusion of variability in D_{LL} for all probability distributions, we see significantly more diffusion than the deterministic solution, with notable variance in ensemble solutions for all variability distributions. The heavier tailed variabilities have denser regions approaching that of the asymptotic solution, and the shape of the KDEs across L-shells is quite distorted contrary to the smoothness seen for a LN D_{LL}. Since there are multiple components of interest in the ensemble results, studies investigating the true underlying probability distribution of ULF wave power are vital to quantifying the shortfall and uncertainty introduced by a deterministic empirical D_{LL} based upon statistical averages.

6. Discussion

In the outer radiation belt, radial diffusion has the ability to both accelerate electrons to relativistic energies and produce fast losses, where the efficiency of the acceleration increases with increasing ULF wave activity (Elkington et al., 2003; Shprits et al., 2008). Many models use an empirical deterministic radial diffusion coefficient dependent on L and K_p, which may sacrifice accuracy (Brautigam & Albert, 2000; Brautigam et al., 2005; Ozeke et al., 2012, 2014). In this paper we present idealized numerical experiments, which investigate the impact of including variability in the radial diffusion equation. Our experiments reintroduce the variability into a parameterized model, where D_{LL} has been binned by Kp. We use the observationally constrained variability in the model to model a variable D_{LL} that reproduces a realistic distribution of values and compare against the constant parameterized value. We employ constant boundary conditions and only study one value of the controlling parameter Kp. In this way, we isolate only the variability of D_{LL} due to its parameterization by Kp.

In all experiments we found that the mean and median of the ensembles exhibit increased diffusion above that for the deterministic approximation. One way to interpret these results is that when the likelihood of strong radial diffusion is large over a particular period (either because the variance in the parameterization is large or because the underlying distribution has a heavy tail), then the diffusion exceeds what one would expect from using a constant diffusion coefficient. It is important to bear in mind that the times where diffusion is weak will not counteract the times when diffusion is strong because there is no means of reversing the diffusion; hence, the periods when diffusion is much stronger than the median will dominate the temporal evolution of the experiment. When the diffusion varies more rapidly, then each member of the ensemble is more likely to contain a period of strong diffusion over the fixed 48-hr experiment length, thus contributing to a stronger diffusion in the mean/median of the ensemble. The ensembles are also sensitive to the size of

the variance (see Experiment 3), again suggesting that it is the likelihood of ensemble members containing periods of very strong diffusion that dominates the ensemble results.

The collected range of numerical experiments suggests that over extended time periods, infrequent instances of very efficient ULF wave-particle interactions make important contributions to radial diffusion and should be included in models in some way. We also note that by using an ensemble framework, the uncertainty in the PSD is explicitly quantified, providing the means to provide a range of confidence in the model for more accurate radiation belt modeling. The quantification of uncertainty in D_{LL} is also important for future data assimilation methods.

Experiment 1 indicates that the amount of diffusion depends upon how rapidly the diffusion coefficient varies. Hence, it is important to understand the timescales of variability. ULF wave power can vary on a range of timescales, which would ideally be accounted for in the radial diffusion coefficient. For example, ULF wave power can increase and persist on the order of tens of minutes during an auroral activation due to substorms (Rae et al., 2011), while decaying on hourly timescales during strong poloidal wave events (Liu et al., 2011). Parameterization of D_{LL} with K_p may therefore not be optimal, since it may not vary quickly enough.

We found that variation of D_{LL} with the added inclusion of local spatial variabilities on a range of length scales resulted in more diffusion that the deterministic solution (see Experiment 2). However, when considering the ensemble averages, all levels of spatial coherence across $L*$ performed similarly. Since applying variability to subglobal spatial scales still allows for an enhanced D_{LL} at several L, this result is somewhat counterintuitive to those found in the other experiments. While it was found that instances of weaker diffusion cannot counteract the temporal evolution imposed by instances of stronger diffusion, counteractions can occur across spatial scales, creating a net diffusion that seems to follow that observed by a globally applied variability. More interestingly, we found that the variance of the possible states in the set of all ensemble solutions decreases significantly with variability applied to increasingly smaller subglobal spatial scales. It is important to understand and quantify these spatial scales. Rae et al. (2019) showed the evolution of ground-based ULF wave power during geomagnetic storms. ULF wave power can exhibit spatial coherence across ranges of L but does not rise and fall everywhere simultaneously due to the complicated evolution of cold plasma density and magnetic field strength in the inner magnetosphere. They also present evidence that the temporal variability of ULF wave power may vary with L. It may also be that spatial coherence varies with time and geomagnetic activity. The spatial variability (in the radial direction) of drift-averaged diffusion due to ULF waves throughout the outer radiation belt promises a rich vein of future work.

Sensitivity of radial diffusion to the variance of the full probabilistic distribution of D_{LL} was explored in Experiment 3. For small variances, the diffusion results approach those of the deterministic model, as expected. But as the variance is increased, the diffusion results rapidly diverge. These results suggest that it is worth seeking alternative parameterizations that focus on variance reduction in the construction of the diffusion model. Another way to reduce the variance in the parameterization may be to focus on the calculation of D_{LL} itself. For example, D_{LL}^E in the Ozeke et al. (2014) model was constructed via a mapping technique that utilized several assumptions: constant (low) wave number $m = 1$, constant width of the wave activity in latitude, and constant ionospheric conductance parameters (Ozeke et al., 2009). These quantities are typically not constant and contribute to the uncertainty in the deterministic model and should be included in the stochastic parameterization. The theoretical background from which D_{LL} is based may also produce uncertainties. Several analytical diffusion rates based on magnetic and electric field assumptions exist, with L dependence ranging from L^6–L^{11} and frequency dependence on a range of wave modes (e.g., Birmingham, 1969; Cornwall, 1968; Elkington et al., 2003; Fälthammar, 1966, 1968; Fei et al., 2006; Schulz & Lanzerotti, 1974). If enough of the underlying variability in the deterministic model is known, the better the variability in the stochastic models can be characterized or accounted for. It should be mentioned however that natural variability might exist, which cannot be parameterized by any means. Deducing levels of natural variability in ULF wave-driven radial diffusion is necessary in understanding information always lost by a deterministic model. If these levels are substantial, our results suggest that a stochastic approach to modeling radial diffusion may be more robust.

The response of radial diffusion to higher likelihoods of an enhanced D_{LL}, which dominates temporal evolutions, was explored in Experiment 4. It is evident that significantly more radial diffusion occurs for heavier
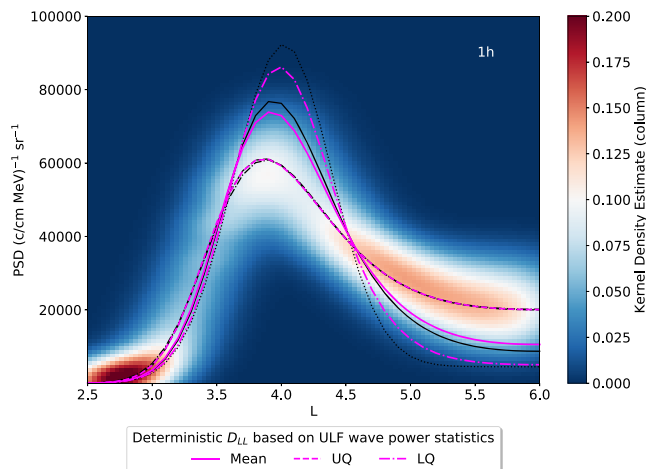
Figure 7. PSD resulting from the radial diffusion equation after 2 days with constant Kp = 3, shown for a constant deterministic D_{LL} based on the mean (solid pink), LQ (dash-dot pink) and UQ (dash pink) of ULF wave power. These plots are laid over the first subplot in Figure 3.

tailed variabilities, indicating that the amount of diffusion is controlled by the relative importance of the large values of D_{LL} in the distribution. A global upper bound for possible ULF wave power is justified since it is counterintuitive for ULF waves to have infinitely large power in a finite-sized magnetosphere. The shape of the distribution is therefore important. It may also be that the shape of the distribution of D_{LL} is not constant. During quiet times when the outer radiation belt is relatively quiescent, the variability might be better represented heavily skewed to the left with a single small upper bound on ULF wave power. In a storm-time model where ULF wave activity is enhanced during the main and recovery phase (Murphy et al., 2011; Murphy et al., 2015; Rae et al., 2011), a right skewed ULF wave power distribution that favors larger ULF wave powers might be more suitable. Further research into tail values of the distribution of ULF wave power is important to constrain the physical upper bound of power variability to include in stochastic models.

In each of our experiments, ensemble averages and KDEs were compared to a (Ozeke et al., 2014) constant deterministic solution, which is based on the median of statistical ULF wave power. However, it may be more fair to compare the evolution of our numerical ensembles with an experiment where D_{LL} is kept constant, but at the mean value of the distribution, especially since the ethos of constructing a diffusion coefficient is to consider the average behavior of the waves. Figure 7 indicates the results of a number of numerical experiments with constant D_{LL} (mean, solid pink; upper quartile, dashed pink; and lower quartile, dash-dot pink) compared with the ensemble result using a LN distribution with $\Delta t = 1$ hr. We observe that the mean-based D_{LL} only causes slightly more diffusion than the median based and is also significantly less diffusive than the ensemble averages. While inclusion of the LQ- and UQ-based D_{LL} does result in a broad span of possible PSD solutions, the UQ produces diffusion only as strong as the ensemble averages, falling short of the regions of highest density seen in the ensemble solutions. It is apparent that having a deterministic representation of D_{LL} fails to represent the underlying distribution of radial diffusion solutions found from the stochastic D_{LL} time series, which better represent the true underlying distribution of ULF wave power. Our ensemble modeling highlights where efforts should be placed to get a better description of D_{LL}, so that we can aim for a parameterization with a quantified uncertainty that truly represents the underlying distribution of possible solutions of the radial diffusion equation.

Diffusion due to other types of wave-particle interactions is important in the outer radiation belt, and similar modeling strategies may be required. Diffusion in pitch angle and energy due to higher-frequency waves is also highly variable (Watt et al., 2019), potentially with different time and length scales depending on location in the magnetosphere. It will be necessary to repeat similar numerical experiments to determine the stochastic parameters necessary to use in stochastic parameterizations of pitch angle and energy diffusion and then design observational analyses that can best constrain those parameters.

7. Conclusions

Our idealized experiments highlight the spatiotemporal impacts of including stochastic parameterizations in the ULF wave-driven radial diffusion. We have shown that diffusion is increased above the deterministic model when the diffusion coefficients vary more rapidly, when the spatial correlation of the diffusion across L-shells ranges from fully coherent to completely independent, and when the variance of the distribution is increased, or a more heavy-tailed distribution is used. We have demonstrated that future research should focus on the temporal evolution of ULF wave power, the spatial correlations of diffusion across L-shells, and the underlying distribution and variance of the radial diffusion coefficients. The successful implementation of a stochastic radial diffusion model requires variability parameters that are derived appropriately; that is, spatial and temporal scales of the variability may themselves vary in time and space. Our research motivates further investigation of stochastic methods for use in radiation belt diffusion models as a method to include the variability of wave-particle interactions in the inner magnetosphere.

Data Availability Statement

Experiment results presented are freely available online (at https://doi.org/10.17864/1947.248).

References

Ali, A. F., Malaspina, D. M., Elkington, S. R., Jaynes, A. N., Chan, A. A., Wygant, J., & Kletzing, C. A. (2016). Electric and magnetic radial diffusion coefficients using the Van Allen probes data. *Journal of Geophysical Research: Space Physics*, *121*, 9586–9607. https://doi.org/10.1002/2016JA023002

Bentley, S. N., Watt, C. E. J., Owens, M. J., & Rae, I. J. (2018). ULF wave activity in the magnetosphere: Resolving solar windinterdependencies to identify driving mechanisms. *Journal of Geophysical Research: Space Physics*, *123*, 2745–2771. https://doi.org/10.1002/2017JA024740

Birmingham, T. J. (1969). Convection electric fields and the diffusion of trapped magnetospheric radiation. *Journal of Geophysical Research*, *74*(9), 2169–2181. https://doi.org/10.1029/JA074i009p02169

Bourdarie, S. A., & Maget, V. F. (2012). Electron radiation belt data assimilation with an ensemble Kalman filter relying on the Salammbo code. *Annales Geophysicae*, *30*(6), 929–943. https://doi.org/10.5194/angeo-30-929-2012

Boyd, A. J., Turner, D. L., Reeves, G. D., Spence, H. E., Baker, D. N., & Blake, J. B. (2018). What causes radiation belt enhancements: A survey of the Van Allen Probes era. *Geophysical Research Letters*, *45*, 5253–5259. https://doi.org/10.1029/2018GL077699

Brautigam, D. H., & Albert, J. M. (2000). Radial diffusion analysis of outer radiation belt electrons during the October 9, 1990, magnetic storm. *Journal of Geophysical Research*, *105*(A1), 291–309. https://doi.org/10.1029/1999JA900344

Brautigam, D. H., Ginet, G. P., Albert, J. M., Wygant, J. R., Rowland, D. E., Ling, A., & Bass, J. (2005). CRRES electric field power spectra and radial diffusion coefficients. *Journal of Geophysical Research*, *110*, A02214. https://doi.org/10.1029/2004JA010612

Christon, S. P., Mitchell, D. G., Williams, D. J., Frank, L. A., Huang, C. Y., & Eastman, T. E. (1988). Energy spectra of plasma sheet ions and electrons from ~50 eV/e to ~1 MeV during plasma temperature transitions. *Journal of Geophysical Research: Space Physics*, *93*(A4), 2562–2572. https://doi.org/10.1029/JA093iA04p02562

Christon, S. P., Williams, D. J., Mitchell, D. G., Huang, C. Y., & Frank, L. A. (1991). Spectral characteristics of plasma sheet ion and electron populations during disturbed geomagnetic conditions. *Journal of Geophysical Research*, *96*(A1), 1–22. https://doi.org/10.1029/90JA01633

Cornwall, J. M. (1968). Diffusion processes influenced by conjugate-point wave phenomena. *Radio Science*, *3*(7), 740–744. https://doi.org/10.1002/rds196837740

Dimitrakoudis, S., Mann, I. R., Balasis, G., Papadimitriou, C., Anastasiadis, A., & Daglis, I. A. (2015). Accurately specifying storm-time ULF wave radial diffusion in the radiation belts. *Geophysical Research Letters*, *42*, 5711–5718. https://doi.org/10.1002/2015GL064707

Drozdov, A. Y., Shprits, Y. Y., Aseev, N. A., Kellerman, A. C., & Reeves, G. D. (2017). Dependence of radiation belt simulations to assumed radial diffusion rates tested for two empirical models of radial transport. *Space Weather*, *15*(1), 150–162. https://doi.org/10.1002/2016SW001426

Elkington, S. R., Hudson, M. K., & Chan, A. A. (2003). Resonant acceleration and diffusion of outer zone electrons in an asymmetric geomagnetic field. *Journal of Geophysical Research*, *108*(A3), 1116. https://doi.org/10.1029/2001JA009202

Fälthammar, C.-G. (1966). On the transport of trapped particles in the outer magnetosphere. *Journal of Geophysical Research*, *71*(5), 1487–1491. https://doi.org/10.1029/JZ071i005p01487

Fälthammar, C.-G. (1968). Radial diffusion by violation of the third adiabatic invariant. In B. M. McCormac (Ed.), *Earth's particles and fields; proceedings of the NATO Advanced Study Institute held at Freising, Germany, July 31-August 11, 1967* (p. 157). New York: Reinhold Book Corporation.

Fei, Y., Chan, A. A., Elkington, S. R., & Wiltberger, M. J. (2006). Radial diffusion and MHD particle simulations of relativisticelectron transport by ULF waves in the September 1998 storm. *Journal of Geophysical Research*, *111*, A12209. https://doi.org/10.1029/2005JA011211

Glauert, S. A., Horne, R. B., & Meredith, N. P. (2014). Simulating the Earth's radiation belts: Internal acceleration and continuous losses to the magnetopause. *Journal of Geophysical Research: Space Physics*, *119*, 7444–7463. https://doi.org/10.1002/2014JA020092

Glauert, S. A., Horne, R. B., & Meredith, N. P. (2018). A 30-year simulation of the outer electron radiation belt. *Space Weather*, *16*, 1498–1522. https://doi.org/10.1029/2018SW001981

Kersten, T., Horne, R. B., Glauert, S. A., Meredith, N. P., Fraser, B. J., & Grew, R. S. (2014). Electron losses from the radiation belts caused by EMIC waves. *Journal of Geophysical Research: Space Physics*, *119*, 8820–8837. https://doi.org/10.1002/2014JA020366

Knutti, R., Furrer, R., Tebaldi, C., & Meehl, G. A. (2010). Challenges in combining projections from multiple climate models. Retrieved from http://www-pcmdi.llnl.gov/ipcc/. https://doi.org/10.1175/2009JCLI3361.1

Kourentzes, N., Barrow, D., & Crone, S. (2014). Neural network ensemble operators for time series forecasting. *Expert Systems with Applications*, *41*, 4235–4244. https://doi.org/10.1016/j.eswa.2013.12.011

Lejosne, S. (2019). Analytic expressions for radial diffusion. *Journal of Geophysical Research: Space Physics*, *124*, 4278–4294. https://doi.org/10.1029/2019JA026786

Lejosne, S., Boscher, D., Maget, V., & Rolland, G. (2013). Deriving electromagnetic radial diffusion coefficients of radiation belt equatorial particles for different levels of magnetic activity based on magnetic field measurements at geostationary orbit. *Journal of Geophysical Research: Space Physics*, *118*, 3147–3156. https://doi.org/10.1002/jgra.50361

Li, Z., Hudson, M., Patel, M., Wiltberger, M., Boyd, A., & Turner, D. (2017). ULF wave analysis and radial diffusion calculation using a global MHD model for the 17 March 2013 and 2015 storms. *Journal of Geophysical Research: Space Physics*, *122*, 7353–7363. https://doi.org/10.1002/2016JA023846

Liu, W., Sarris, T. E., Li, X., Zong, Q.-G., Ergun, R., Angelopoulos, V., & Glassmeier, K. H. (2011). Spatial structure and temporal evolution of a dayside poloidal ULF wave event. *Geophysical Research Letters*, *38*, L19104. https://doi.org/10.1029/2011GL049476

Liu, W., Tu, W., Li, X., Sarris, T., Khotyaintsev, Y., Fu, H., et al. (2016). On the calculation of electric diffusion coefficient of radiation belt electrons with in situ electric field measurements by THEMIS. *Geophysical Research Letters*, *43*, 1023–1030. https://doi.org/10.1002/2015GL067398

Lyons, L. R., & Thorne, R. M. (1973). Equilibrium structure of radiation belt electrons. *Journal of Geophysical Research*, *78*(13), 2142–2149. https://doi.org/10.1029/JA078i013p02142

Maget, V., Sicard-Piet, A., Bourdarie, S., Lazaro, D., Turner, D. L., Daglis, I. A., & Sandberg, I. (2015). Improved outer boundary conditions for outer radiation belt data assimilation using THEMIS-SST data and the Salammbo-EnKF code. *Journal of Geophysical Research: Space Physics*, *120*, 5608–5622. https://doi.org/10.1002/2015JA021001

Mann, I. R., Lee, E. A., Claudepierre, S. G., Fennell, J. F., Degeling, A., Rae, I. J., et al. (2013). Discovery of the action of a geophysical synchrotron in the Earths Van Allen radiation belts. *Nature Communications*, *4*, 2795. https://doi.org/10.1038/ncomms3795

Meredith, N. P., Horne, R. B., Glauert, S. A., & Anderson, R. R. (2007). Slot region electron loss timescales due to plasmaspheric hiss and lightning-generated whistlers. *Journal of Geophysical Research*, *112*, A08214. https://doi.org/10.1029/2007JA012413

Murphy, K. R., Mann, I. R., Rae, I. J., Sibeck, D. G., & Watt, C. E. J. (2016). Accurately characterizing the importance of wave-particle interactions in radiation belt dynamics: The pitfalls of statistical wave representations. *Journal of Geophysical Research: Space Physics*, *121*, 7895–7899. https://doi.org/10.1002/2016JA022618

Murphy, K. R., Mann, I. R., & Sibeck, D. G. (2015). On the dependence of storm time ULF wave power on magnetopause location: Impacts for ULF wave radial diffusion. *Geophysical Research Letters*, *42*, 9676–9684. https://doi.org/10.1002/2015GL066592

Murphy, K. R., Rae, I. J., Mann, I. R., & Milling, D. K. (2011). On the nature of ULF wave power during nightside auroral activations and substorms: 1. Spatial distribution. *Journal of Geophysical Research*, *116*, A00I21. https://doi.org/10.1029/2010JA015757

Olifer, L., Mann, I. R., Ozeke, L. G., Rae, I. J., & Morley, S. K. (2019). On the relative strength of electric and magnetic ULF wave radial diffusion during the March 2015 geomagnetic storm. *Journal of Geophysical Research: Space Physics*, *124*, 2569–2587. https://doi.org/10.1029/2018JA026348

Ozeke, L. G., Mann, I. R., Murphy, K. R., Degeling, A. W., Claudepierre, S. G., & Spence, H. E. (2018). Explaining the apparent impenetrable barrier to ultra-relativistic electrons in the outer Van Allen belt. *Nature Communications*, *9*(1), 1844. https://doi.org/10.1038/s41467-018-04162-3

Ozeke, L. G., Mann, I. R., Murphy, K. R., Jonathan Rae, I., & Milling, D. K. (2014). Analytic expressions for ULF wave radiation belt radial diffusion coefficients. *Journal of Geophysical Research: Space Physics*, *119*, 1587–1605. https://doi.org/10.1002/2013JA019204

Ozeke, L. G., Mann, I. R., Murphy, K. R., Rae, I. J., Milling, D. K., Elkington, S. R., et al. (2012). ULF wave derived radiation belt radial diffusion coefficients. *Journal of Geophysical Research*, *117*, A04222. https://doi.org/10.1029/2011JA017463

Ozeke, L. G., Mann, I. R., Murphy, K. R., Sibeck, D. G., & Baker, D. N. (2017). Ultra-relativistic radiation belt extinction and ULF wave radial diffusion: Modeling the September 2014 extended dropout event. *Geophysical Research Letters*, *44*, 2624–2633. https://doi.org/10.1002/2017GL072811

Ozeke, L. G., Mann, I. R., & Rae, I. J. (2009). Mapping guided Alfvén wave magnetic field amplitudes observed on the ground to equatorial electric field amplitudes in space. *Journal of Geophysical Research*, *114*, A01214. https://doi.org/10.1029/2008JA013041

Perry, K. L., Hudson, M. K., & Elkington, S. R. (2005). Incorporating spectral characteristics of Pc5 waves into three-dimensional radiation belt modeling and the diffusion of relativistic electrons. *Journal of Geophysical Research*, *110*, A03215. https://doi.org/10.1029/2004JA010760

Rae, I. J., Murphy, K. R., Watt, C. E. J., & Mann, I. R. (2011). On the nature of ULF wave power during nightside auroral activations and substorms: 2. Temporal evolution. *Journal of Geophysical Research*, *116*, A00I22. https://doi.org/10.1029/2010JA015762

Rae, I. J., Murphy, K. R., Watt, C. E. J., Sandhu, J. K., Georgiou, M., Degeling, A. W., et al. (2019). How do ultra-low frequency waves access the inner magnetosphere during geomagnetic storms? *Geophysical Research Letters*, *46*, 10,699–10,709. https://doi.org/10.1029/2019GL082395

Reeves, G. D., Chen, Y., Cunningham, G. S., Friedel, R. W. H., Henderson, M. G., Jordanova, V. K., et al. (2012). Dynamic radiation environment assimilation model: DREAM. *Space Weather*, *10*, S03006. https://doi.org/10.1029/2011SW000729

Riley, P., & Wolf, R. A. (1992). Comparison of diffusion and particle drift descriptions of radial transport in the Earth's inner magnetosphere. *Journal of Geophysical Research*, *97*(A11), 16,865–16,876. https://doi.org/10.1029/92JA01538

Roederer, J. G. (1970). *Dynamics of geomagnetically trapped radiation / J.G. Roederer.* Berlin: Springer-Verlag.

Roederer, J. G., & Zhang, H. (2014). *Dynamics of magnetically trapped particles* (Vol. 403). Berlin, Heidelberg: Springer. https://doi.org/10.1007/978-3-642-41530-2

Schulz, M., & Lanzerotti, L. (1974). Particle diffusion in the radiation belts / [by] M. Schulz [and] L. J. Lanzerotti. Springer-Verlag Berlin.

Shin, D.-K., & Lee, D.-Y. (2013). Determining radial boundary conditions of outer radiation belt electrons using THEMIS observations. *Journal of Geophysical Research: Space Physics*, *118*, 2888–2896. https://doi.org/10.1002/jgra.50334

Shprits, Y. Y., Elkington, S. R., Meredith, N. P., & Subbotin, D. A. (2008). Review of modeling of losses and sources of relativistic electrons in the outer radiation belt I: Radial transport. *Journal of Atmospheric and Solar-Terrestrial Physics*, *70*(14), 1679–1693. https://doi.org/10.1016/j.jastp.2008.06.008

Shprits, Y. Y., Thorne, R. M., Reeves, G. D., & Friedel, R. (2005). Annales Geophysicae Radial diffusion modeling with empirical lifetimes: comparison with CRRES observations. (Vol. 23; Tech. Rep.)

Thorne, R. M., Li, W., Ni, B., Ma, Q., Bortnik, J., Chen, L., et al. (2013). Rapid local acceleration of relativistic radiation-belt electrons by magnetospheric chorus. *Nature*, *504*, 411. https://doi.org/10.1038/nature12889

Tu, W., Elkington, S. R., Li, X., Liu, W., & Bonnell, J. (2012). Quantifying radial diffusion coefficients of radiation belt electrons based on global MHD simulation and spacecraft measurements. *Journal of Geophysical Research*, *117*, A10210. https://doi.org/10.1029/2012JA017901

Ukhorskiy, A. Y., Sitnov, M. I., Takahashi, K., & Anderson, B. J. (2009). Radial transport of radiation belt electrons due to stormtime Pc5 waves. *Annales Geophysicae*, *27*(5), 2173–2181. https://doi.org/10.5194/angeo-27-2173-2009

Vacaresse, A., Boscher, D., Bourdarie, S., Blanc, M., & Sauvaud, J. A. (1999). Modeling the high-energy proton belt. *Journal of Geophysical Research*, *104*(A12), 28,601–28,613. https://doi.org/10.1029/1999JA900411

Watt, C. E. J., Allison, H. J., Meredith, N. P., Thompson, R. L., Bentley, S. N., Rae, I. J., et al. (2019). Variability of quasilinear diffusion coefficients for plasmaspheric hiss. *Journal of Geophysical Research: Space Physics*, *124*, 8488–8506. https://doi.org/10.1029/2018JA026401

Watt, C. E. J., Rae, I. J., Murphy, K. R., Anekallu, C., Bentley, S. N., & Forsyth, C. (2017). The parameterization of wave-particle interactions in the Outer Radiation Belt. *Journal of Geophysical Research: Space Physics*, *122*, 9545–9551. https://doi.org/10.1002/2017JA024339

Welling, D., Koller, J., & Camporeale, E. (2011). Verification of SpacePy's radial diffusion radiation belt model. *Geoscientific Model Development*, *5*, 277–287. https://doi.org/10.5194/gmdd-4-2165-2011